Mon. Not. R. Astron. Soc. **345,** 1015–1029 (2003)

WIYN Open Cluster Study – XVI. Optical/infrared photometry and comparisons with theoretical isochrones

Aaron J. Grocholski⋆ and Ata Sarajedini⋆

Department of Astronomy, University of Florida, PO Box 112055, Gainesville, FL 32611, USA

Accepted 2003 July 16. Received 2003 July 14; in original form 2003 June 5

ABSTRACT

We present combined optical/near-infrared photometry (*BVIK*) for six open clusters – M35, M37, NGC 1817, NGC 2477, NGC 2420 and M67. The open clusters span an age range from 150 Myr to 4 Gyr and have metal abundances from [Fe/H] = −0.27 to +0.09 dex. We have utilized these data to test the robustness of theoretical main sequences constructed by several groups as denoted by the following designations – Padova, Baraffe, Y^2, Geneva and Siess. The comparisons of the models with the observations have been performed in the [M_V, $(B-V)_0$], [M_V, $(V-I)_0$] and [M_V, $(V-K)_0$] colour–magnitude diagrams as well as the distance-independent [$(V-K)_0$, $(B-V)_0$] and [$(V-K)_0$, $(V-I)_0$] two-colour diagrams. We conclude that none of the theoretical models reproduces the observational data in a consistent manner over the magnitude and colour range of the unevolved main sequence. In particular, there are significant zero-point and shape differences between the models and the observations. We speculate that the crux of the problem lies in the precise mismatch between theoretical and observational colour–temperature relations. These results underscore the importance of pursuing the study of stellar structure and stellar modelling with even greater intensity.

Key words: stars: evolution – stars: fundamental parameters – Hertzsprung–Russell (HR) diagram – stars: late-type – open clusters and associations: general.

1 INTRODUCTION

With the possible exception of the white dwarf cooling sequence, the main sequence is perhaps the best understood phase of stellar evolution. Conversion of hydrogen to helium occurs in the stellar core, representing a stable and long-lasting phase of evolution. As we proceed along the main sequence from high-mass stars to low-mass, the production of energy in the core transitions from the CNO bi-cycle to the proton–proton chain, while, at the same time, the primary energy transfer mechanism in the core goes from convection to radiative diffusion. In addition, the outer convection zone deepens progressively until the star becomes fully convective below $\sim$0.35 $M_\odot$ (Baraffe et al. 1998). All of these features are modelled with varying degrees of success in modern stellar structure and evolution codes.

The *degree* of success that we attribute to stellar models is primarily based on how well they match the observations. Comparisons such as this have been performed in a number of ways. One method that has been used in the past involves comparing isochrones with the locations of nearby field stars in the Hertzsprung–Russell (HR) diagram (e.g. Baraffe et al. 1998; Bergbusch & VandenBerg 2001; Yi et al. 2001). Aside from the uncertainties inherent in their trigonometric parallaxes, the primary drawback of using these stars to test the isochrones is the need to correct their colours for their differing metallicities.

Another method that has been used to test the theoretical isochrones is exemplified by the work of Andersen et al. (1991) and Nordström & Johansen (1994), and most recently by Lastennet & Valls-Gabaud (2002, and references therein). These authors have determined the masses, effective temperatures and luminosities of individual stars in nearby binary systems, and compared their HR diagram locations with the predictions of theoretical models. While the method has a number of intrinsic advantages, its primary shortcoming is the obvious requirement that stars must be in binary systems and in relative proximity to the Sun to be studied in detail.

A third method used to test theoretical stellar models, and the one that we are utilizing in the present work, involves comparing the theoretical isochrones with *cluster* colour–magnitude diagrams (CMDs) and two-colour diagrams (TCDs) in various passbands (e.g. Castellani et al. 2002; von Hippel et al. 2002; von Hippel, Sarajedini & Ruiz 2003). Since all stars are of the same age and metal abundance, this approach is less uncertain than comparing with individual field stars; however, the reddening is still required to perform the comparisons in the TCD (although the similarity in the slopes of the reddening vector and the model loci mitigates this somewhat), and both the distance and the reddening are needed for the CMD comparisons. With the veritable explosion of recent high-quality

⋆E-mail: aaron@astro.ufl.edu (AJG); ata@astro.ufl.edu (AS)

Table 1. Open cluster information.

Name	Available photometry	Log age	$E(B-V)$	[Fe/H]
M35 (NGC 2168)	$UBVRIJHK_S$	8.17	0.19	−0.160
M37 (NGC 2099)	$\ldots BV\ldots JHK_S$	8.73	0.27	0.089
NGC 1817	$\ldots BVRIJHK_S$	8.80	0.26	−0.268
NGC 2477	$UBV\ldots IJHK_S$	9.04	0.23	0.019
NGC 2420	$\ldots BVRIJHK_S$	9.24	0.05	−0.266
M67 (NGC 2682)	$UBVRIJHK_S$	9.60	0.04	0.000

Table 2. Open cluster distance moduli.

Cluster	Padova	Baraffe	Geneva	Y^2	Siess	Twarog et al.
M35 (NGC 2168)	10.16	10.41	9.81	9.91	9.96	10.30
M37 (NGC 2099)	11.55	11.40	11.50	11.35	11.75	11.55
NGC 1817	12.10	12.30	11.90	11.85	12.00	12.15
NGC 2477	11.55	11.60	11.30	11.15	11.45	11.55
NGC 2420	12.12	12.45	11.95	11.90	12.07	12.10
M67 (NGC 2682)	9.80	9.80	9.60	9.45	9.65	9.80

CCD photometry for open clusters, this technique is becoming increasingly more powerful as we will demonstrate in the present work.

This paper is organized as follows. Section 2 presents a discussion of the optical and infrared photometry. We briefly compare and contrast the various stellar evolution models in Section 3. Section 4 represents the primary scientific results of the present investigation; herein, we discuss the successes and failures of the models in terms of how well they match the TCDs and CMDs of open clusters. Finally, we summarize our results in Section 5.

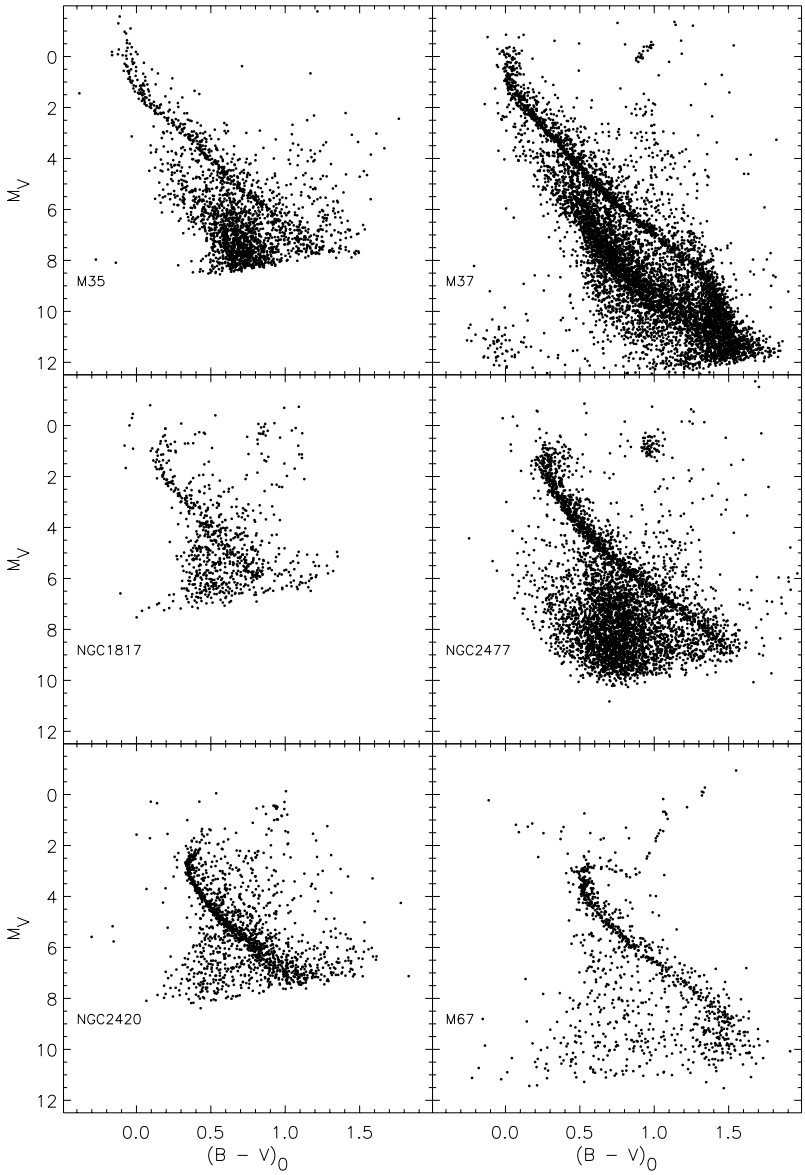

Figure 1. CMDs in the $[M_V, (B-V)_0]$ plane for the six clusters in our data set. The distance moduli and reddenings are given in Table 1. All plots have the same axis scale and the clusters are presented in order from youngest (top left) to oldest (lower right).

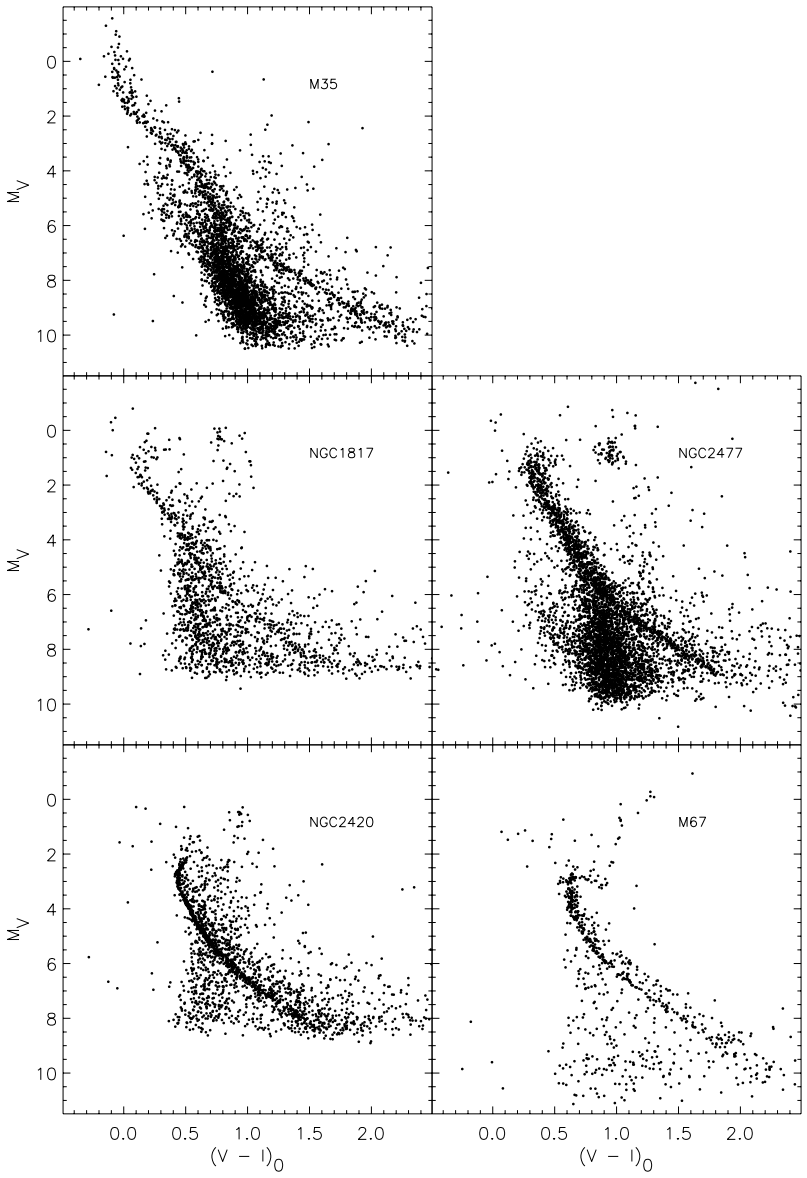

Figure 2. As Fig. 1 except that the CMDs are in the $[M_V, (V - I)_0]$ plane. We note that M37 is not included because Kalirai et al. (2001) do not include I-band photometry in their data set.

2 OBSERVATIONAL DATA

The optical photometry for the six open clusters considered herein is taken from the following sources: M35, NGC 2420, NGC 1817 – WIYN Open Cluster Study (Deliyannis et al., in preparation); M67 – Montgomery, Marschall & Janes (1993); M37 – Kalirai et al. (2001); and NGC 2477 – Kassis et al. (1997). To complement the optical data, we utilize JHK_S infrared photometry available from the Second Incremental Data Release of the Two Micron All Sky Survey (2MASS) Point Source Catalog.[1] For all clusters in our sample we use the same criteria for the 2MASS data retrieval. First, source brightness is limited to sixth magnitude or fainter because of the possible saturation of bright sources (Carpenter 2000). Secondly, we have initially chosen all cluster samples to have a radius of 30 arcmin. The radius is then reduced to as small as 10 arcmin so as to isolate cluster members and minimize field star contamination. Lastly, the 2MASS catalogue provides a read flag (rd_flg) which indicates how photometry of each star was measured. We have excluded from our sample any sources marked with a read flag of zero in any one band, since this implies that the star was not detected in that band and the magnitude reported is therefore only an upper limit. We note that a majority of source magnitudes come from point spread function fitting (rd_flg = 2); however, we have chosen to include stars with aperture photometry (rd˙flg =1) so as to allow the inclusion of brighter cluster stars.

The 2MASS programme uses a K-short (K_S) filter for their photometry, which we have chosen to convert to the Bessell & Brett (1988) (hereafter BB) K-band using the transformation equations derived by Carpenter (2001) adapted as follows:

$$(J - K_{BB}) = [(J - K_S) - (-0.011 \pm 0.005)]/(0.972 \pm 0.006) \quad (1)$$

[1] http://irsa.ipac.caltech.edu/

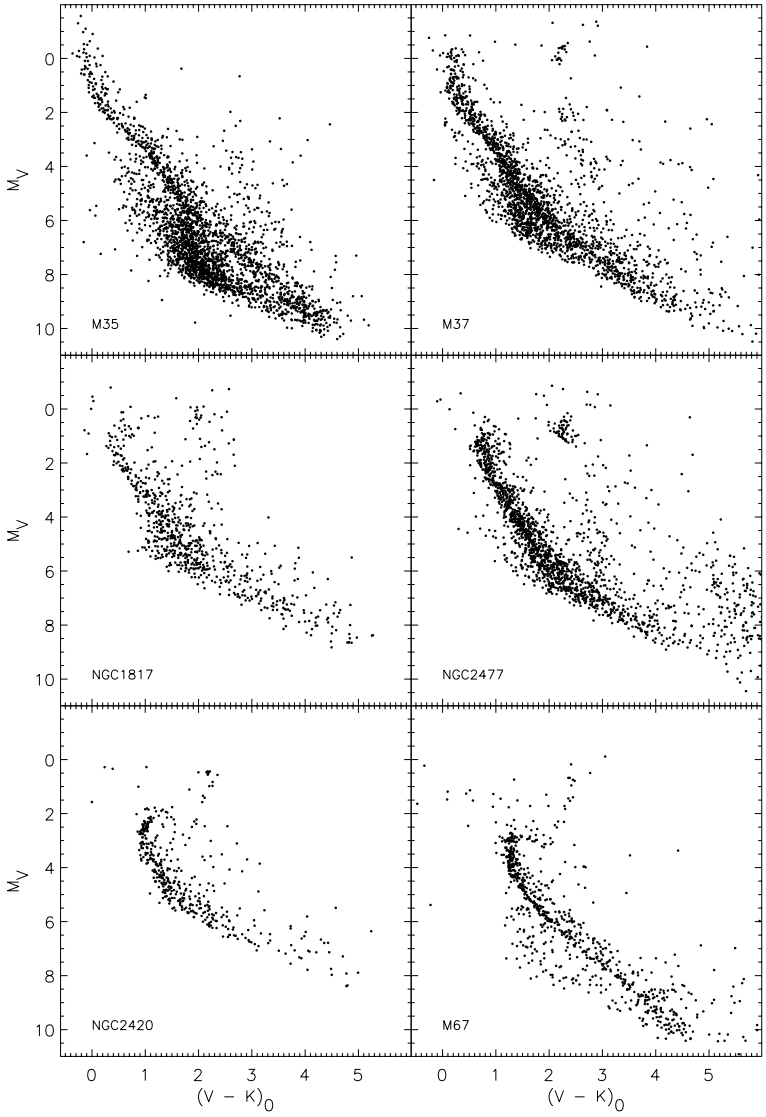

Figure 3. As Fig. 1 except that the CMDs are in the $[M_V, (V - K)_0]$ plane. It is evident from the plots that the CMDs are limited by the depth of the K-band data.

Table 3. Theoretical model input parameters.

	Padova	Baraffe	Geneva	Y^2	Siess
Opacity	OPAL (1993)[a]	OPAL (1996)[b]	OPAL (?)[c]	OPAL (1996)[b]	OPAL (1996)[b]
Low-temperature opacity	AF94	AF94	AF94, Kurucz (1991)	AF94	AF94
Equation of state	$T > 10^7$: Kippenhahn[d] $T < 10^7$: MHD[e]	SCVH[f]	Maeder & Meynet (1989)	OPAL (1996)[b]	based on Pols et al. (1995)
Core overshoot	$0.25H_p$ for $M \geqslant 1.5$ M$_\odot$	None	$0.2H_p$ for $M \geqslant 1.5$ M$_\odot$	$0.2H_p$ for age $\leqslant$ 2Gyr	$0.2H_p$ for $Z = 0.02$ (all others = 0)
Mixing length, α	1.68	1.9	1.6	1.7431	1.605
He abundance	$Y_p = 0.23$	$Y_{solar} = 0.282$	$Y_p = 0.24$	$Y_p = 0.23$	$Y_p = 0.235$
He enrichment, $\frac{\Delta Y}{\Delta Z}$	2.25	n/a	2.5 for $Z > 0.02$ 3 for $Z \leqslant 0.02$	2.0	2.0
Synthetic photometry	ATLAS9[g] DUSTY99[h] Fluks et al. (1994)	NextGen[i]	BaSeL-2.2[j]	BaSeL-2.2[j]	Siess et al. (1997)

[a]Iglesias & Rogers (1993). [b]Iglesias & Rogers (1996). [c]Geneva isochrones were published over the course of several years and as such utilize OPAL opacities from different years. See Lejeune & Schaerer (2001) for more information. [d]Kippenhahn, Thomas & Weigert (1965). [e]Mihalas et al. (1990). [f]Saumon, Chabrier & VanHorn (1995). [g]Castelli, Gratton & Kurucz (1997). [h]Chabrier et al. (2000). [i]Hauschildt et al. (1999). [j]Westera, Lejeune & Buser (1999).

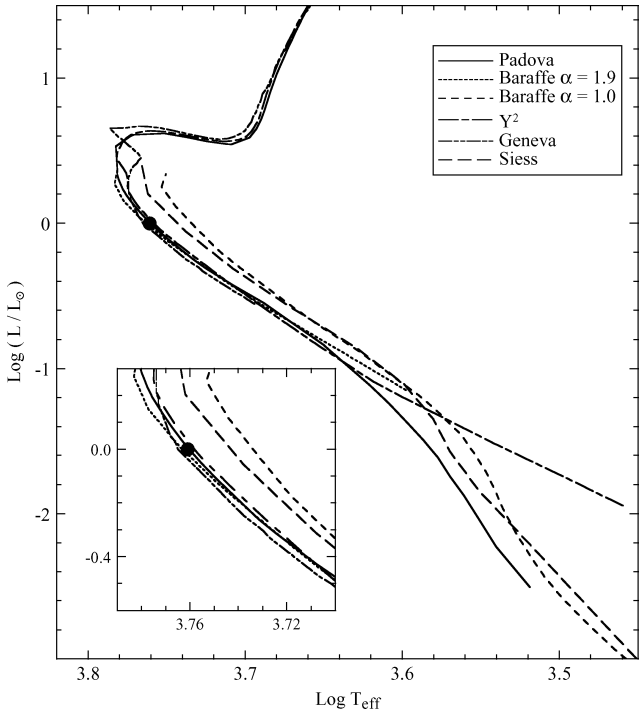

Figure 4. We plot $\log(L/\mathrm{L}_{\odot})$ versus $\log(T_{\rm eff})$ for each of the models used in this study. All isochrones are for solar metallicity at an age of 5 Gyr. The position of the Sun is marked by the filled circle. The inset shows a close-up of the region around the Sun's location.

and

$$K_{\rm BB} = [K_{\rm S} - (-0.044 \pm 0.003)] - (0.000 \pm 0.005)(J - K_{\rm BB}). \quad (2)$$

The BB photometric system has been adopted by a majority of the stellar evolutionary models analysed in the present paper.

We combine optical and infrared photometry for stars in each cluster that are common to both data sets. All photometry files have RA and Dec. available for each star. To combine the data, we calculate the spatial offset between each star in the infrared data set and every star listed in the corresponding optical data set. When the spatial offset is minimized to within a given threshold, the two stars are considered a match. The threshold distance is chosen based on the combined RA and Dec. errors and turns out to be 2.8 arcsec for all clusters.

Twarog, Ashman & Anthony-Twarog (1997) have compiled a data base of information for 76 open clusters, for which they provide internally consistent values of reddening, distance modulus and metallicity. All of the clusters discussed in this study are included in the Twarog et al. (1997) catalogue, so we choose to adopt their values for the reddening and metallicity. Cluster ages are taken from Grocholski & Sarajedini (2002). In the case of M35, its age is calculated using the method described in Grocholski & Sarajedini (2002), which involves adopting ages from the WEBDA[2] data base and offsetting them to the age scale of Sarajedini (1999). We note that, while we have tried to make the cluster ages as internally consistent as possible, small variations in age have no effect on the location of theoretical isochrones along the unevolved main sequence. Table 1 lists these cluster parameters along with the filter passbands of the available photometry.

[2] http://obswww.unige.ch/webda/webda.html

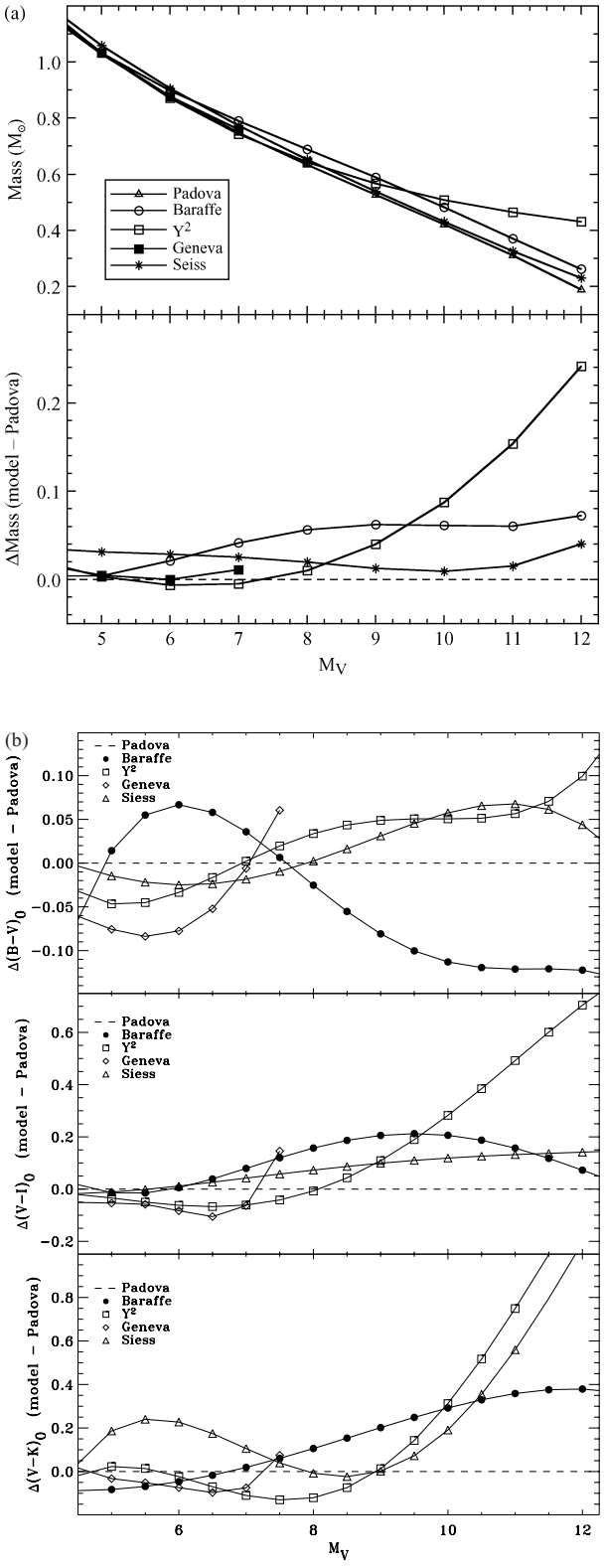

Figure 5. (a) The upper panel shows the relationship between absolute magnitude in the V band and stellar mass in units of solar masses for each of the models considered herein. In the lower panel, we have arbitrarily selected the Padova isochrones as the reference and plot the mass difference between each set of models and this reference. (b) In these three panels we plot the difference in colour between each model and the solar-abundance Padova isochrones as a function of absolute V-band magnitude for $(B-V)_0$ (top panel), $(V-I)_0$ (middle) and $(V-K)_0$ (bottom).

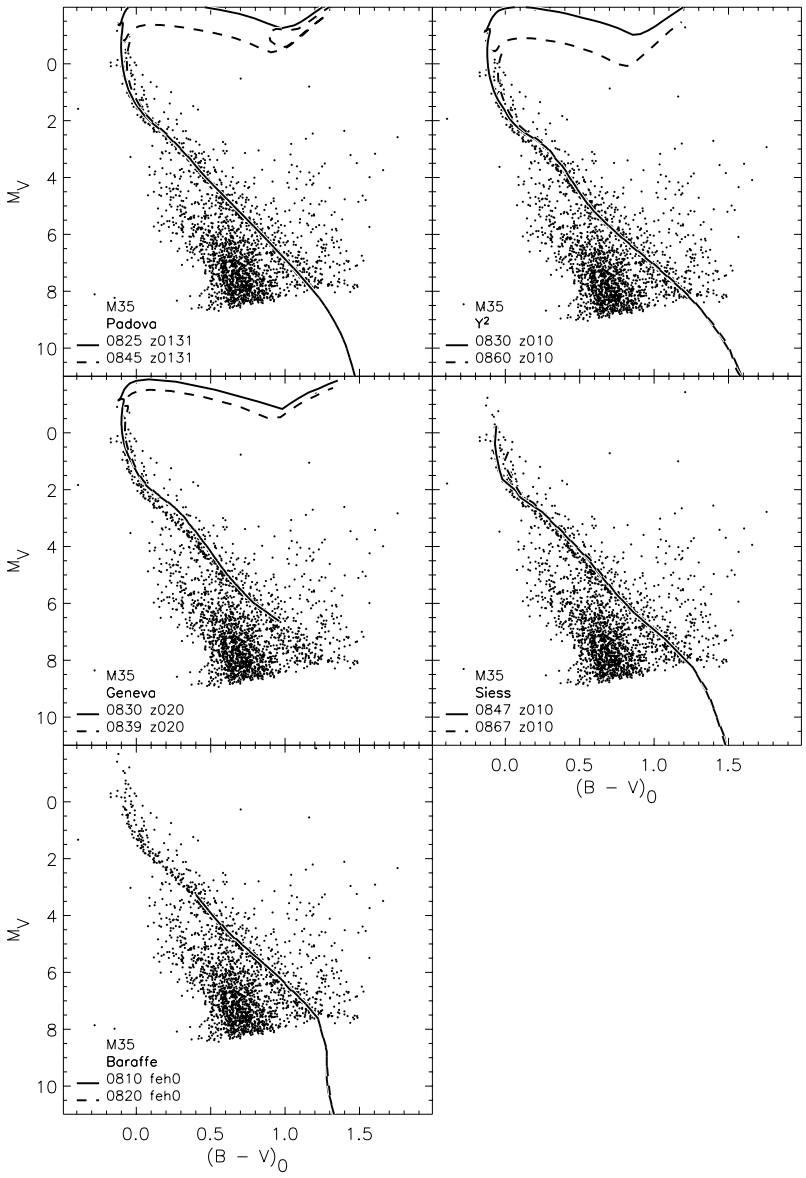

Figure 6. Comparisons between the $[M_V, (B-V)_0]$ CMD of M35 and theoretical models from the Padova, Y^2, Geneva and Siess groups. Note that the cluster distance modulus has been adjusted so that the models and observations agree at $M_V = 6.0$ in the *VI* CMDs. The logarithms of the plotted ages are given along with the metal abundance (Z) of the models.

Since we are primarily interested in comparing theoretical isochrones with cluster photometry in a variety of passbands, we have chosen to determine the distance moduli in the following manner. Given the adopted reddenings in Table 1, we shift each set of isochrones (described in Section 3) vertically in the $(V-I)_0$ CMD until the model main sequence at $M_V = 6.0$ fits that of the clusters. Since M37 does not have *I*-band data, we utilize $(V-K)_0$ for the main-sequence fitting. We have avoided using $(B-V)_0$ for this purpose because it is more sensitive than $(V-I)_0$ to metallicity variations at temperatures above ∼4000 K ($M_V \sim 8.5$) which could result in erroneous distance determinations in cases where the closest available isochrone metallicity differs somewhat from the actual cluster abundance (Baraffe, private communication). The results, along with the distances given by Twarog et al. (1997), are given in Table 2. In this way, we can be sure that the models fit the main sequences in one colour at a given point, allowing us to investigate how well they fit in other colours at other points along the main sequence.

To correct for interstellar extinction, we adopt the reddening law derived by Cardelli, Clayton & Mathis (1989), with which, using their value of $R_V = 3.1$ and taking into account the central wavelength of each filter, we find the following relations for the near-infrared passbands: $A_J = 0.282A_V$, $A_H = 0.180A_V$ and $A_K = 0.116A_V$. For observations of M37, $A_B = 1.41A_V$, and for all other optical photometry, $A_U = 1.57A_V$, $A_B = 1.35A_V$, $A_R = 0.839A_V$ and $A_I = 0.560A_V$.

In Figs 1 and 2 we present $[M_V, (B-V)_0]$ and $[M_V, (V-I)_0]$ CMDs, respectively, for all clusters using the full optical data and in Fig. 3 we show $[M_V, (V-K)_0]$ CMDs using the combined optical and infrared data sets. The clusters are plotted in order of increasing

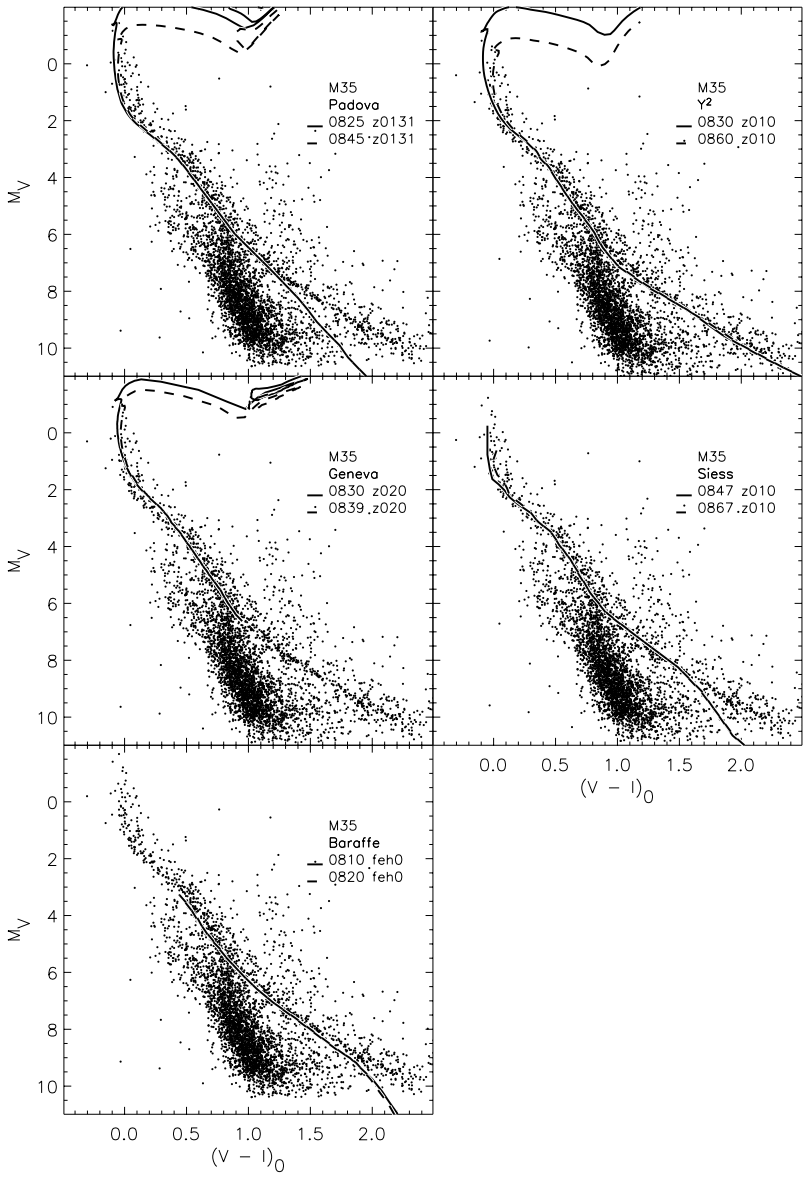

Figure 12. Comparisons between the $[M_V, (V - I)_0]$ CMD of M35 and theoretical models from the Padova, Y^2, Geneva, Siess and Baraffe groups. The logarithms of the plotted ages are given along with the metal abundance (Z) of the models.

age from upper left to lower right. We remind the reader that M37 does not have I-band observations available and is not included in Fig. 2.

3 THEORETICAL MODELS

We now introduce and briefly compare the five sets of theoretical isochrones that are used in the present analysis – Padova (Girardi et al. 2002),[3] Baraffe (Baraffe et al. 1998),[4] Y^2 (Yi et al. 2001),[5] Geneva (Lejeune & Schaerer 2001)[6] and Siess (Siess, Dufour & Forestini 2000).[7] While we do not intend this to be a comprehensive review of the stellar models, we point out some of the similarities and differences between the input parameters of the five groups as listed in Table 3.

With respect to the opacities, all of the groups use versions of the OPAL opacities (e.g. Iglesias & Rogers 1996) for high temperatures, supplemented by the Alexander & Ferguson (1994, AF94) tables for low temperatures. The only caveat is that the Geneva models also consider the Kurucz (1991) low-temperature opacities. We see that all five groups utilize different sources for their equations of state. Three of the groups use similar values for core overshoot in all of their models, while Siess has only included overshoot for their solar metallicity models. Baraffe has chosen not to include core overshoot because the focus of their work is low-mass stars, which,

[3] http://pleiadi.pd.astro.it/∼lgirardi/isoc_photsys.html
[4] See reference list for anonymous FTP instructions.
[5] http://www.astro.yale.edu/demarque/yyiso.html
[6] http://webast.ast.obs-mip.fr/stellar/
[7] http://www-laog.obs.ujf-grenoble.fr/activites/starevol/evol.html

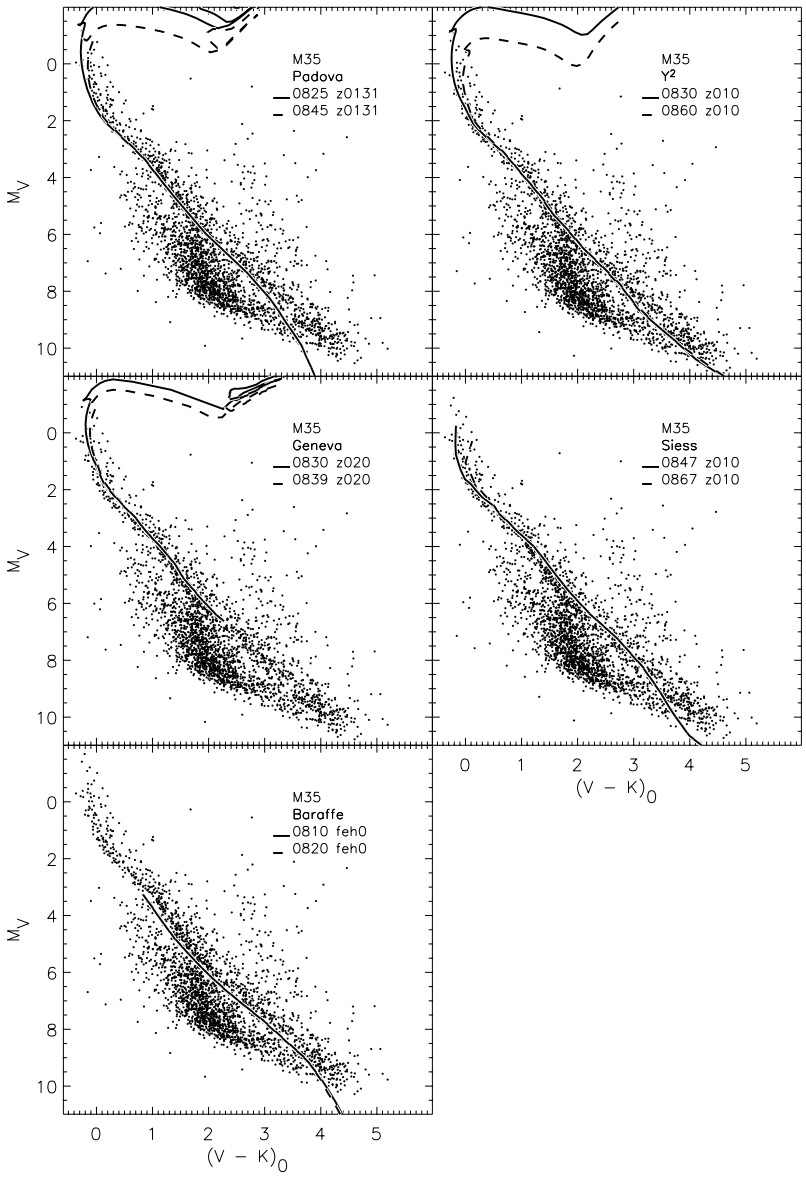

Figure 17. Comparisons between the $[M_V, (V-K)_0]$ CMD of M35 and theoretical models from the Padova, Y^2, Geneva, Siess and Baraffe groups. The logarithms of the plotted ages are given along with the metal abundance (Z) of the models.

for masses below $\sim$0.35 $M_\odot$, are fully convective so an overshoot parameter is not necessary. Also, for low-mass stars above this limit, a convective core is only present for a small fraction of time during their evolution, so inclusion of overshoot will not have a significant effect on these objects (Chabrier & Baraffe 1997). Mixing length parameters are similar for all groups, varying by less than 20 per cent. It is important to keep in mind that the Baraffe models are available with three mixing length values, $\alpha = 1.0$, 1.5 and 1.9. Setting the mixing length equal to 1.9 is required to match observations of the Sun (Baraffe et al. 1998); however, these models are not extended below 0.6 $M_\odot$ ($M_V \sim 8.8$). Baraffe et al. (1998) find that, for $M \leqslant 0.6\ M_\odot$, their isochrones with the three different mixing lengths converge, implying that the mixing length has little effect on the models below this mass. As such, we combine the $\alpha = 1.9$ models for masses above $\sim$0.6 $M_\odot$ with $\alpha = 1.0$ models covering the very low-mass stars.

Lastly, we compare each group's method of deriving synthetic photometry for their models which is then used to convert effective temperatures to colours. The calculations by both the Geneva and Y^2 groups come from versions of the BaSeL stellar spectral library (see e.g. Lejeune & Schaerer 2001). This library is based on model atmosphere spectra by Kurucz (private communication in Lejeune, Cuisinier & Buser 1997), Fluks et al. (1994) and Bessell et al. (1989, 1991). Padova calibrations are also based largely on the spectral library of Kurucz (1992) with extension to cool stars through the use of the Fluks et al. (1994) empirical M giant spectra and the DUSTY99 (Chabrier et al. 2000) atmosphere models of cool dwarf (type M and later) synthetic spectra [see section 3 of Girardi et al. (2002) for a complete discussion]. The Siess model uses $T_{\rm eff}$–BC relations from Schmidt-Kaler (1982) and Bessell (1991), and $T_{\rm eff}$–colour relationships from Fitzgerald (1970) and Arribas & Martinez-Roger (1988, 1989). Lastly, the Baraffe isochrones use stellar spectra generated

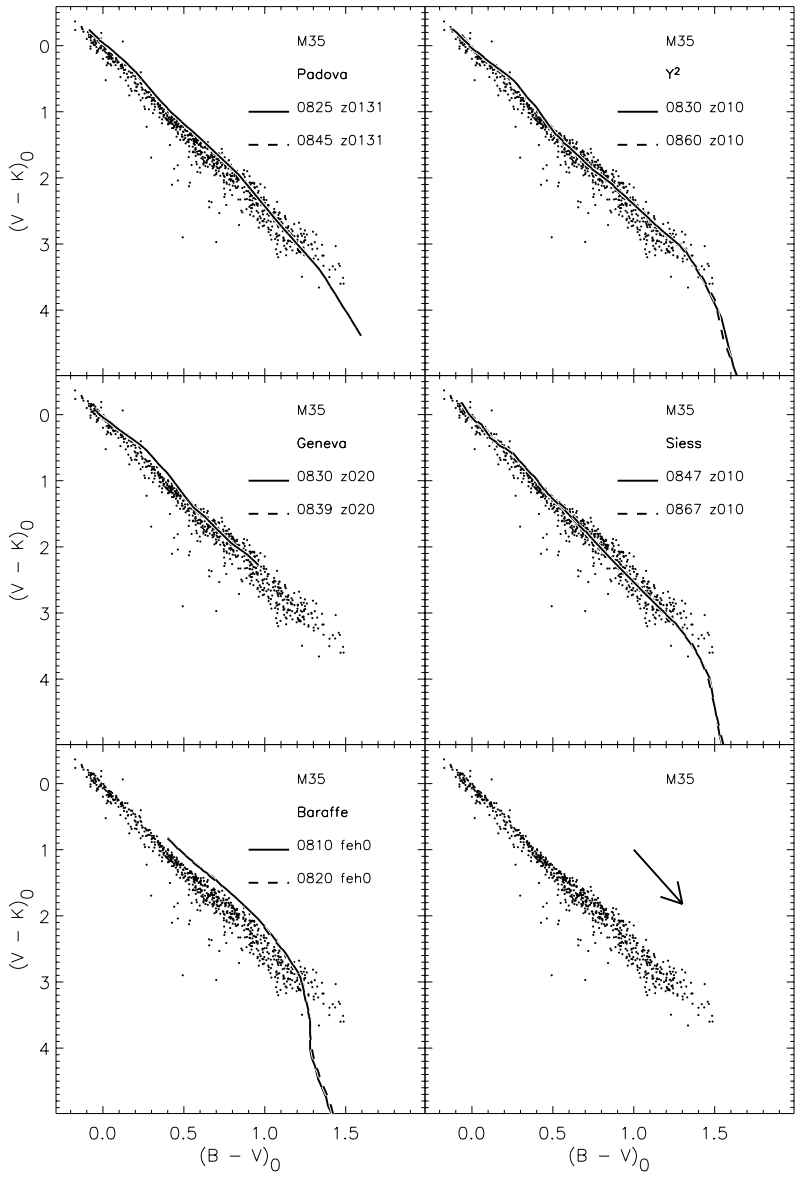

Figure 23. TCDs using $(B-V)_0$ and $(V-K)_0$ data for main-sequence stars in M35. The solid lines represent the models indicated in each panel. These plots show that, even when we remove the uncertainties inherent in the distance moduli, the theoretical isochrones still do not reproduce the shape of the observed sequence in the TCD. We have included a reddening vector with length $(B-V)_0 = 0.3$.

with the NEXTGEN model atmosphere code (e.g. Hauschildt, Allard & Baron 1999) which is a predecessor of the aforementioned DUSTY99 models.

In Fig. 4 we plot $\log(L/L_{\rm Sun})$ versus $\log(T_{\rm eff})$ for each of the models used in this study (note that we have included the complete $\alpha = 1.0$ as well as the $\alpha = 1.9$ Baraffe models). All isochrones are for solar metallicity and an age of 5 Gyr; the position of the Sun is indicated by the filled circle. The inset box shows a close-up of the region around the Sun. Comparing the models in the theoretical plane allows us to eliminate the uncertainty inherent in the transformation to the observational plane. In this figure we see that four of the plotted isochrones, Padova (solid line), Baraffe, $\alpha = 1.9$ (short-dashed line), Y^2 (long–short-dashed line) and Geneva (double-dot–dashed line) are all in good agreement for the upper main sequence and the position of the Sun, but show considerable deviation beginning around 0.1 $L_\odot$ ($M_V \sim 7.5$, 0.65 $M_\odot$, $T_{\rm eff} \sim$ 4100 K, and spectral type ∼K7). Neither Siess nor Baraffe ($\alpha = 1.0$) matches the Sun and, for a given luminosity, predicts cooler effective temperatures than the other isochrones on the upper main sequence.

Fig. 5(a) displays the relationship between model mass and absolute magnitude in the V band. In particular, the lower panel of Fig. 5(a) shows the difference in mass between each isochrone and the Padova set, which has been chosen as an arbitrary reference. We see that the mass differences are minimized at $M_V \sim 6.0$, the magnitude at which we have determined the distance modulus of each cluster (Section 2). At fainter magnitudes the differences between the various models steadily increase but are generally less than 0.1 $M_\odot$. Fainter than $M_V \sim 9$, the masses of the Y^2 models begin to deviate from the others. As we discuss how well the models fit the observations in the CMD, Fig. 5(a) will prove useful in estimating the mass at each value of the absolute magnitude.

Fig. 5(b) compares the difference in colour between each model and the solar-abundance Padova isochrone as a function of absolute

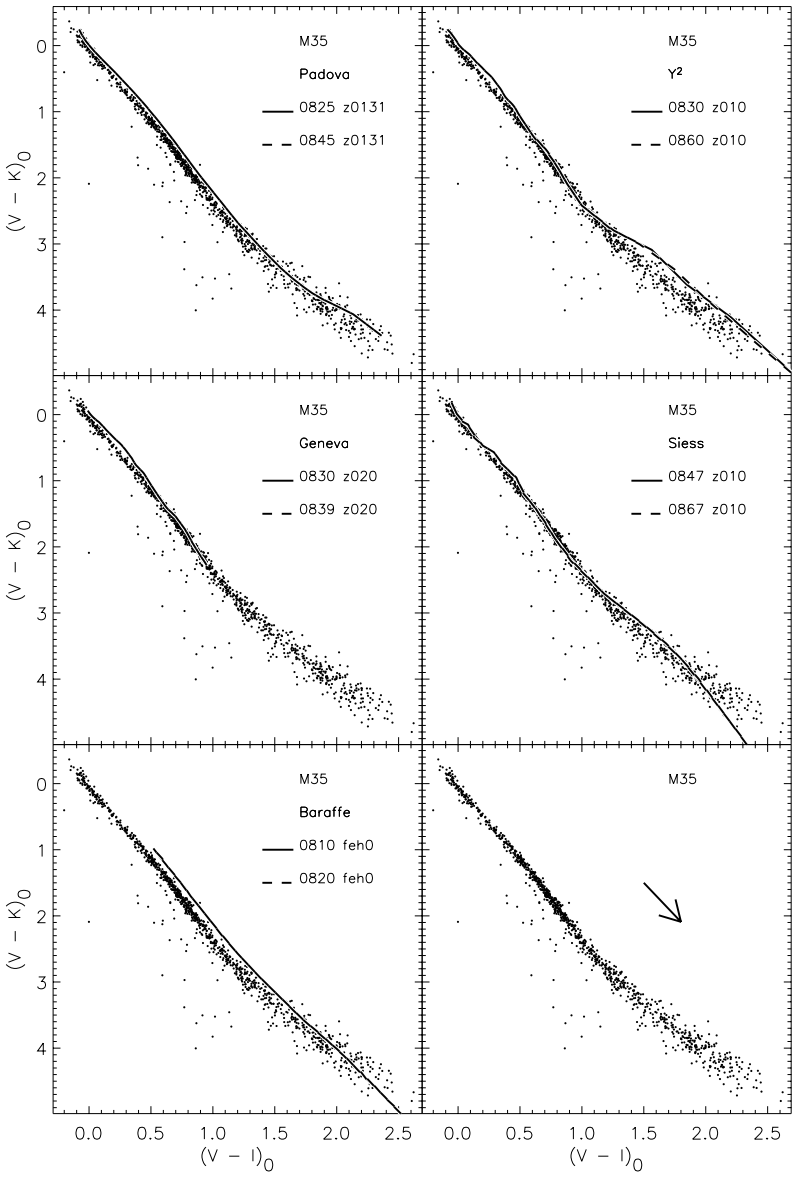

Figure 29. As Fig. 23, except that TCDs using $(V - I)_0$ and $(V - K)_0$ data are plotted. The reddening vector shown has length $(V - I)_0 = 0.3$.

V-band magnitude for $(B - V)_0$ (top panel), $(V - I)_0$ (middle) and $(V - K)_0$ (bottom). As with Fig. 5(a), the colour differences are generally smaller at $M_V \sim 6.0$ and increase at fainter magnitudes. Furthermore, one would expect that if the models all used the same method for converting effective temperatures to colours, then the appearance of Fig. 5(b) would be solely a reflection of the differences in the physics of the models (see Fig. 4). We see, however, that this is not the case; there are no clear systematic trends in these differences from model to model (with the possible exception of the Geneva isochrones). These virtually random differences indicate that the disagreement between models is a result of both the chosen physics and the colour transformations.

4 RESULTS

4.1 Colour–magnitude diagrams

As mentioned in Section 1, we are interested in comparing the observational CMDs with theoretical models for a variety of colours. These comparisons are illustrated in Figs 6–22[8] for the six clusters in our sample. In each case, we show the $[M_V, (B - V)_0]$, $[M_V, (V - I)_0]$ and $[M_V, (V - K)_0]$ diagrams along with the isochrone that is closest to the metallicity of the cluster as listed in Table 1. Listed in each plot are the cluster name and model name, along with two numbers that indicate which isochrone is used. The first number gives the log age of the model [e.g. 0945 → log(age] = 9.45) and the second indicates the metal abundance (e.g. z019 → $Z = 0.019$). In the case of the Padova isochrones, Leo Girardi kindly provided interpolated models that match the cluster metal abundances. In addition, because the M37 data of Kalirai et al. (2001) do not possess I-band photometry, we only show data in the $(B - V)_0$ and $(V - K)_0$ colours. To simplify the discussion below, we will refer to mismatches between the models and the observations as occuring in

[8] Only a sample of these CMDs (Figs 6, 12 and 17) are included in the printed version of this paper. The rest are available from http://www.blackwell-publishing.com/products/journals/suppmat/mnr/mnr7028/mnr7028sm.htm

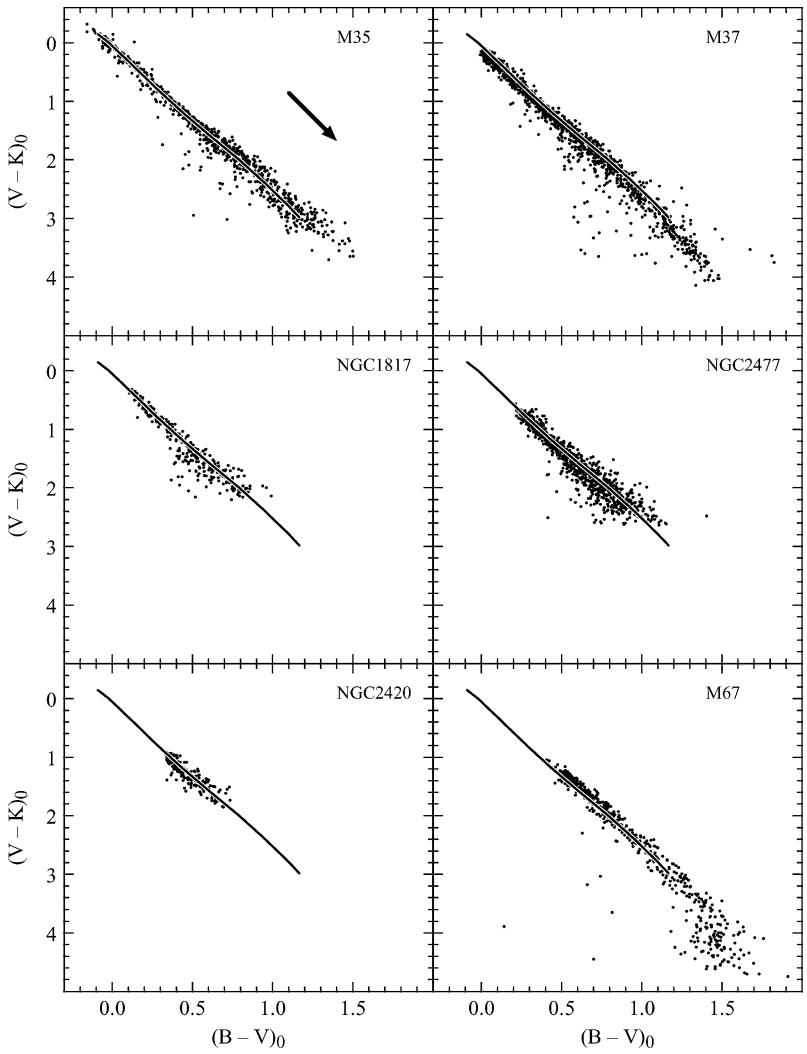

Figure 34. TCDs using $(B - V)_0$ and $(V - K)_0$ data for all of the clusters in the present study compared with the observed sequence for M35 (solid line). We have included a reddening vector with length $(B - V)_0 = 0.3$.

the magnitude direction with the understanding that there may be a component in the colour direction as well.

Looking at the CMD and isochrone comparisons in Figs 6–22 , a number of trends stand out. First, we confirm that all of the models fit the cluster main sequence at $M_V = 6.0$ in the $(V - I)_0$ plane. This is to be expected given the manner in which we determined the cluster distance moduli. Next, we examine the isochrone comparisons in the $(B - V)_0$ plane shown in Figs 6–11 . In the vast majority of cases, the model main sequences match the observations at $M_V = 6.0$ adequately. There are two notable exceptions to this. First, the M37 photometry is significantly fainter than all of the isochrones considered herein by between ∼0.5 and ∼0.9 mag in colour. As such, we will exclude it from further discussion within the context of the other $(B - V)_0$ CMDs. Secondly, the Baraffe models are consistently brighter than the observations at $M_V = 6.0$, except in the case of M35. Moving on to the other regions of the CMD in the $(B - V)_0$ plane, all of the models reproduce the unevolved main sequence in the range $2.0 \lesssim M_V \lesssim 7.0$ reasonably well. The primary exception to this is the fit of the Geneva models to the M35 photometry shown in the middle left panel of Fig. 6. In this case, the main sequence of the isochrone is clearly offset from the observed one for $M_V \lesssim 5.0$. Another exception, although not as obvious, is apparent in the comparison between the Y^2 models and the M35 data in the upper right panel of Fig. 6. Again, the isochrone is brighter than the data in the range $2.0 \lesssim M_V \lesssim 5.0$. Thirdly, there is the comparison between NGC 2420 and the Siess models in Fig. 10 where the theoretical main sequence lies above the data. It is unclear what causes these mismatches. However, in the case of the Geneva models, it may be a result of the fact that the cluster (M35) metallicity is lower than those used in the isochrones. For the clusters with photometry extending reliably below $M_V \sim 8.0$ (NGC 2477 and M67, again excluding M37), we find that the Padova and Baraffe models diverge the most from the observed main sequences, while the Y^2 and Siess models deviate the least. Note that the Geneva model MS does not extend faint enough for this comparison to be made.

Moving on to a consideration of the $[M_V, (V - I)_0]$ diagrams in Figs 12–16, we see a similar behaviour in the range $2.0 \lesssim M_V \lesssim 7.0$ as noted in the case of the $(B - V)_0$ CMDs. In short, all of the models perform reasonably well in matching the observed main sequences. The difficulties arise in the magnitude ranges fainter than $M_V \sim 8.0$; the Padova models diverge the most from the

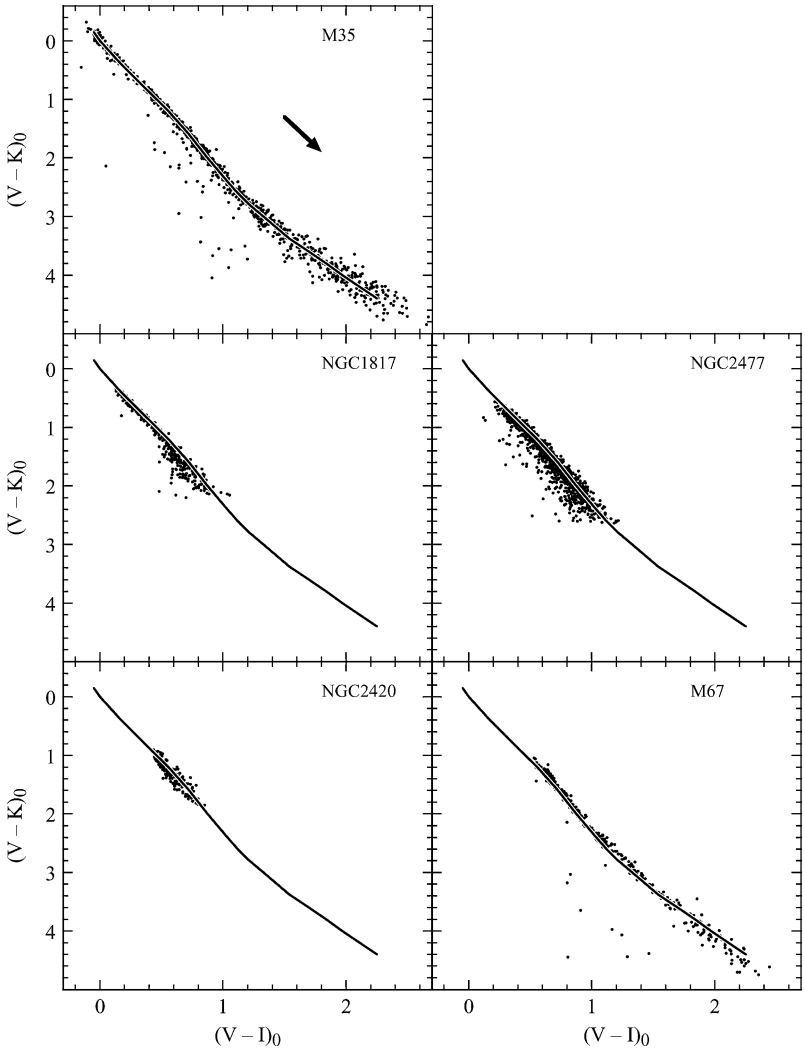

Figure 35. TCDs using $(V - I)_0$ and $(V - K)_0$ data for all of the clusters in the present study compared with the observed sequence for M35 (solid line). We have included a reddening vector with length $(V - I)_0 = 0.3$.

cluster main sequences, while the Baraffe theoretical main sequences reproduce the observed ones more consistently than any of other sets.

Lastly, we examine the $[M_V, (V - K)_0]$ diagrams which were constructed by matching optical photometry with 2MASS near-infrared photometry. We note that the level of agreement between the isochrones and the data at $M_V = 6.0$ is not consistent from cluster to cluster and model to model. With the exception of M37 where the distance fits have been performed in the $[M_V, (V - K)_0]$ plane, in most cases, the model main sequences are fainter than the observed ones. However, the Padova main sequence matches that of M35 at $M_V = 6.0$; similarly, the Geneva models match the main sequence of NGC 2477 at $M_V = 6.0$. In terms of the level of overall agreement along the main sequence, we can say that, like the $(B - V)_0$ and $(V - I)_0$ CMDs, the $(V - K)_0$ models perform better in the range $2.0 \lesssim M_V \lesssim 7.0$ as compared with fainter magnitudes. However, with the exception of M35, the models are generally fainter than the observational main sequences.

To conclude this section, we note that *none* of the theoretical models fits the unevolved main sequence (i.e. $M_V \gtrsim 4$) adequately in all three colours. Either the shape of the isochrone does not match the observations or the location does not match, or both. The small difference between the metallicity of the isochrones and the observations is unlikely to be the cause of this mismatch.

4.2 Two-colour diagrams

One of the ways in which we can eliminate the use of the distance modulus in the present analysis is to compare the optical/infrared photometry of open clusters with theoretical isochrones in the TCD. In this plane, only the reddenings of the clusters are required, allowing us to investigate further the robustness of the models. Figs 23–28 show the $[(V - K)_0, (B - V)_0]$ TCDs, while Figs 29–33[9] display the $[(V - K)_0, (V - I)_0]$ TCDs for main-sequence stars in our sample of open clusters. The arrow in each figure represents the slope of the reddening vector $[E(B - V) = E(V - I) = 0.3]$ which is roughly parallel to the two-colour sequence, suggesting that inferences made from these diagrams are largely insensitive to the adopted reddenings.

[9] Again, only a sample of these figures (Figs 23 and 29) are shown in the printed version of the paper, while the remainder are available from http://www.blackwellpublishing.com/products/journals/suppmat/mnr/mnr7028/mnr7028sm.htm

Looking first at the $[(V-K)_0, (B-V)_0]$ diagrams, except in a minority of cases, there is a zero-point offset between the theoretical two-colour sequence and the observations; the models are too blue in $(V-K)_0$ at a given $(B-V)_0$ as compared with the observational data. In addition, the detailed shapes of the theoretical sequences can be dramatically different from the data, especially in the case of the Baraffe models for $(V-K)_0 \gtrsim 3.0$. The M37 and M67 data, which extend to the reddest colours, nicely underscore these shape differences. Largely similar conclusions (i.e. models are offset to bluer colours and do not reproduce the shape of the observed TCDs) can be reached by examining the $[(V-K)_0, (V-I)_0]$ diagrams.

As a sanity check on the observations, Figs 34 and 35 present TCDs of each cluster compared with the sequence for M35 determined by eye using the data in the upper left panels. A reddening vector equal to $E(B-V) = E(V-I) = 0.3$ is also shown in each figure. We see that, in most cases, the positions and shapes of the two-colour sequences for each cluster are in good accord with that of M35. In Fig. 34, the data for M37 are below the M35 line by $\sim$0.1 mag; this may account for the fact that in the $[M_V, (B-V)_0]$ CMDs (Fig. 7), the M37 data are shifted away from the isochrones by a significant amount as compared with the data from the other clusters. Fig. 34 also shows that the M67 two-colour data appear to be slightly offset from the M35 sequence in the colour range $0.5 \lesssim (B-V)_0 \lesssim 1.0$. Lastly, in Fig. 35, we see that the M67 sequence has a slightly different shape as compared with the M35 $[(V-K)_0, (V-I)_0]$ line. Taken together, the TCDs in Figs 34 and 35 provide reassurance that the observational data we have considered herein are internally consistent.

5 CONCLUSION

We have presented combined optical/near-infrared photometry for six open clusters. The optical data have been obtained as part of the WIYN Open Cluster Study and taken from the literature, while the near-infrared observations are from the Second Incremental Data Release of the Two Micron All Sky Survey Point Source Catalog. The open clusters span an age range from 150 Myr to 4 Gyr and have metal abundances from [Fe/H] $= -0.27$ to $+0.09$ dex. We have utilized these data to test the robustness of theoretical main sequences constructed by several groups as denoted by the following designations – Padova (Girardi et al. 2002), Baraffe (Baraffe et al. 1998), Y^2 (Yi et al. 2001), Geneva (Lejeune & Schaerer 2001) and Siess (Siess et al. 2000). The comparisons of the models with the observations have been performed in the $[M_V, (B-V)_0]$, $[M_V, (V-I)_0]$ and $[M_V, (V-K)_0]$ CMDs, as well as the distance-independent $[(V-K)_0, (B-V)_0]$ and $[(V-K)_0, (V-I)_0]$ TCDs. The reddenings have been taken from Twarog et al. (1997) and the distance moduli were determined by adopting these reddenings and then matching each isochrone to the observed main sequences at $M_V = 6.0$ in the $[M_V, (V-I)_0]$ plane ($[M_V, (V-K)_0]$ for M37).

We conclude that none of the theoretical models reproduces the observational data in a consistent manner over the magnitude and colour range of the unevolved main sequence. In particular, there are significant zero-point and shape differences between the models and the observations. In the CMDs, most of the models performed reasonably well for stars with mass $\gtrsim$0.75 $M_\odot$, but did not do so for stars with lower masses. In the TCDs, the theoretical sequences are too blue in $(V-K)_0$ at a given $(B-V)_0$ and $(V-I)_0$ as compared with the observational data. The shapes of the theoretical sequences can also be dramatically different as compared with the data. From Figs 4 and 5 we can say with a fair amount of certainty that the crux of the problem lies in the precise mismatch between theoretical and observational colour–temperature relations. Depending on how these relations are derived, one of the problems could be missing sources of opacity in the atmospheres of the model stars. These results underscore the importance of pursuing the study of stellar structure and stellar modelling with even greater intensity.

ACKNOWLEDGMENTS

The authors are grateful to Isabelle Baraffe, Pierre Demarque and Ted von Hippel for providing comments on an early version of this manuscript, and to Tom Kehoe for helping with the preparation of the manuscript. AJG is especially indebted to Isabelle Baraffe for many enlightening discussions. The authors are appreciative of Glenn Tiede for his countless contributions. We thank Con Deliyannis, Kent Montgomery and Jason Kalirai for supplying us with electronic copies of their photometry, and Leo Girardi for providing models for previously unpublished metallicities. We also acknowledge the referee, Bruce Twarog, for comments that greatly improved the presentation of this paper. This publication makes use of data products from the Two Micron All Sky Survey, which is a joint project of the University of Massachusetts and the Infrared Processing and Analysis Centre/California Institute of Technology, funded by the National Aeronautics and Space Administration and the National Science Foundation. This research was supported by NSF CAREER grant AST 00-94048 and grant AST 01-96212.

REFERENCES

Alexander D. R., Ferguson J. W., 1994, ApJ, 437, 879 (AF94)
Andersen J., Clausen J. V., Nordström B., Tomkin J., Mayor M., 1991, A&A, 246, 99
Arribas S., Martinez Roger C., 1988, A&A, 206, 63
Arribas S., Martinez Roger C., 1989, A&A, 215, 305
Baraffe I., Chabrier G., Allard F., Hauschildt P. H., 1998, A&A, 337, 403 (Baraffe)
Bergbusch P. A., VandenBerr D. A., 2001, ApJ, 556, 322
Bertelli G., Bressan A., Chiosi C., Fagotto F., Nasi E., 1994, A&AS, 106, 275
Bessell M. S., , 1991, AJ, 101, 662
Bessell M. S., Brett J. M., 1988, PASP, 100, 1134 (BB)
Bessell M. S., Brett J. M., Scholz M., Wood P. R., 1989, A&AS, 77, 1
Bessell M. S., Brett J. M., Scholz M., Wood P. R., 1991, A&AS, 89, 335
Cardelli J. A., Clayton G. C., Mathis J. S., 1989, ApJ, 345, 245
Carpenter J. M., 2000, AJ, 120, 3139
Carpenter J. M., 2001, AJ, 121, 2851
Castellani V., Degl'Innocenti S., Prada Moroni P. G., Tordiglione V., 2002, MNRAS, 334, 193
Castelli F., Gratton R. G., Kurucz R. L., 1997, A&A, 318, 841
Chabrier G., Baraffe I., 1997, A&A, 327, 1039
Chabrier G., Baraffe I., Allard F., Hauschildt P. H., 2000, ApJ, 542, 464
Fitzgerald M. P., 1970, A&A, 4, 234
Fluks M. A., Plez B., The P. S., de Winter D., Westerlund B. E., Steenman H. C., 1994, A&AS, 105, 311
Girardi L., Bertelli G., Bressan A., Chiosi C., Groenewegen M. A. T., Marigo P., Salasnich B., Weiss A., 2002, A&A, 391, 195 (Padova)
Grocholski A. J., Sarajedini A., 2002, AJ, 123, 1603
Hauschildt P. H., Allard F., Baron E., 1999, ApJ, 512, 377
Iglesias C. A., Rogers F. J., 1993, ApJ, 412, 752
Iglesias C. A., Rogers F. J., 1996, ApJ, 464, 943
Kalirai J. S., Ventura P., Richer H. B., Fahlman G. G., Durrell P. R., D'Antona F., Marconi G., 2001, AJ, 122, 3239
Kassis M., Janes K. A., Friel E. D., Phelps R. L., 1997, AJ, 113, 1723
Kippenhahn R., Thomas H.-C., Weigert A., 1965, Z. Astrophys., 61, 241
Kurucz R. L., 1991, in Crivellari L., Hubeny I., Hummer D. G., eds, NATO ASI Series C, Vol. 341, Stellar Atmospheres: Beyond Classical Models. Kluwer, Dordrecht, p. 441

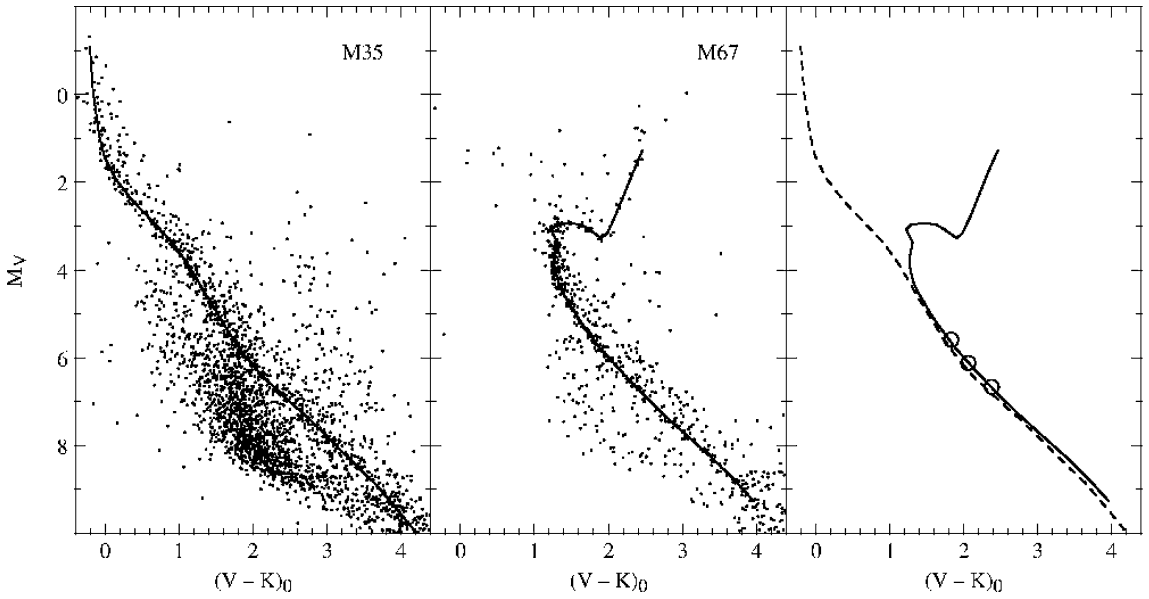

Figure A1. The $[M_V, (V-K)_0]$ CMDs for M35 and M67 with the solid lines representing the fiducial sequences drawn by eye through the highest density of points. The right-hand panel shows the fiducials for both clusters plotted in the same plane along with field stars (open circles) from Percival et al. (2003) with close-to-solar abundances and *Hipparcos* parallaxes.

Table A1. Cluster fiducials.

M35		M67	
V	$V-K$	V	$V-K$
9.0	0.32	11.0	2.57
9.5	0.34	11.5	2.44
10.0	0.36	12.0	2.32
10.5	0.40	12.5	2.20
11.0	0.44	12.9	2.09
11.5	0.51	13.0	2.01
12.0	0.66	12.8	1.85
12.5	0.89	12.7	1.74
13.0	1.17	12.65	1.58
13.5	1.45	12.7	1.40
14.0	1.66	12.8	1.33
14.5	1.83	13.1	1.42
15.0	2.01	13.2	1.41
15.5	2.19	13.4	1.38
16.0	2.39	13.5	1.375
16.5	2.64	13.6	1.374
17.0	2.96	13.7	1.385
17.5	3.29	13.8	1.40
18.0	3.59	14.0	1.43
18.5	3.89	14.2	1.48
19.0	4.19	14.4	1.55
19.5	4.44	14.6	1.62
20.0	4.69	14.8	1.69
		15.0	1.77
		15.5	1.99
		16.0	2.26
		16.5	2.54
		17.0	2.84
		17.5	3.17
		18.0	3.50
		18.5	3.80
		19.0	4.07

Kurucz R. L., 1992, in Barbuy B., Renzini A., eds, Stellar Populations of Galaxies. Kluwer, Dordrecht, p. 225
Lastennet E., Valls-Gabaud D., 2002, A&A, 396, 551
Lejeune T., Schaerer D., 2001, A&A, 366, 538 (Geneva)
Lejeune T., Cuisinier F., Buser R., 1997, A&AS, 125, 229
Maeder A., Meynet G., 1989, A&A, 210, 155
Mihalas D., Hummer D. G., Mihalas B. W., Däppen W., 1990, ApJ, 350, 300
Montgomery K. A., Marschall L. A., Janes K. A., 1993, AJ, 106, 181
Nordström B., Johansen K. T., 1994, A&A, 291, 777
Percival S. M., Salaris M., Kilkenny D., 2003, A&A, 400, 541
Pols O. R., Tout C. T., Eggleton P. P., Han Z., 1995, MNRAS, 274, 964
Sarajedini A., 1999, AJ, 118, 2321
Saumon D., Chabrier G., VanHorn H. M., 1995, ApJS, 99, 713
Schmidt-Kaler T., 1982, in Schaifers K., Voigt H. H., eds, Landolt-Börnstein New Series, Vol. 2b, Astronomy and Astrophysics – Stars and Star Clusters. Springer-Verlag, New York
Siess L., Forestini M., Dougados C., 1997, A&A, 324, 556
Siess L., Dufour E., Forestini M., 2000, A&A, 358, 593 (Siess)
Twarog B. A., Ashman K. M., Anthony-Twarog B. J., 1997, AJ, 114, 2556
von Hippel T., Steinhauer A., Sarajedini A., Deliyannis C. P., 2002, AJ, 124, 1555
von Hippel T., Sarajedini A., Ruiz M. T., 2003, ApJ, 595, 794
Westera P., Lejeune T., Buser R., 1999, in Hubeny I., Heap S., Cornett R., eds, ASP Conf. Ser. Vol. 192, Spectrophotometric Dating of Stars and Galaxies. Astron. Soc. Pac., San Francisco, p. 203
Yi S., Demarque P., Kim Y.-C., Lee Y.-K., Ree C., Lejeune T., Barnes S., 2001, ApJS, 136, 417 (Y^2)

APPENDIX A: CLUSTER $V-K$ FIDUCIAL SEQUENCES

Published $(V-K)_0$ fiducial sequences are rare for open clusters; as such, to help fill an important need, we have derived such sequences for the youngest (M35) and oldest (M67) clusters in our sample. The left-hand and centre panels of Fig. A1 show our adopted fiducial sequences for M35 and M67, respectively. These have been constructed by eye through the highest density of points in the CMD and are given in Table A1. The cluster data and the fiducials are plotted after accounting for the effects of reddening (Table 1) and distance using the median of the values in Table 2. The right-hand panel in Fig. A1 shows the two fiducials plotted together to reinforce the point that the observations of these clusters agree well with each other even to the limits of the M67 photometry at $M_V \sim 9$.

To investigate how well solar-abundance field main-sequence stars compare with these two clusters, we have combined optical photometry of field stars with [Fe/H] values within ± 0.1 of the Sun and *Hipparcos* parallaxes from table 1 of Percival, Salaris & Kilkenny (2003) with K-band data for these same stars from the Second Incremental Data Release of the 2MASS Point Source Catalog. The open circles in the right-hand panel of Fig. A1 represent three stars that meet these criteria. It is evident that there is good agreement between the locations of the field stars and the main-sequence locations of M35 and M67.

This paper has been typeset from a TEX/LATEX file prepared by the author.